



# Manifold regularized deep canonical variate analysis with interpretable attribute guidance for three-phase flow process monitoring

Linghan Li <sup>a</sup>, Feng Dong <sup>a,b</sup>, Shumei Zhang <sup>a,\*</sup>

<sup>a</sup> Tianjin Key Laboratory of Process Measurement and Control, School of Electrical and Information Engineering, Tianjin University, Tianjin, China

<sup>b</sup> School of Information and Intelligent Engineering, Tianjin Renai College, Tianjin, China

## ARTICLE INFO

### Keywords:

Oil-gas-water three-phase flow  
Process monitoring  
Canonical variate analysis (CVA)  
Deep neural networks (DNN)  
Manifold regularization  
Attribute learning

## ABSTRACT

Oil-gas-water three-phase flow has multiple flow states, exhibiting dynamic, nonlinear, and instantaneous behaviors. Monitoring and analysis of flow state are crucial for ensuring safe operation of industrial processes. However, the absence of a universal definition for three-phase flow states, owing to the complex flow characteristics and structures, leads to that labeling three-phase flow states by categories is impractical. For comprehensive monitoring and analysis, the flow states should be described from both global (e.g., the dominant phase) and local (e.g., the interphase structure) aspects. Given the aforementioned challenges, the work aims to address the accurate identification of typical three-phase flow states and to meticulously monitor and analyze the continuous evolutionary process of three-phase flow. To achieve it, the manifold regularized deep canonical variate analysis with attribute guidance (Ag-MRDCVA) is proposed, which not only introduces an innovative monitoring paradigm that designs state attributes for process description but also facilitates knowledge transfer from typical flow states to transition states. For enhancing the model's feature embedding capabilities, an attribute guidance module is introduced to increase supervision information at both class and attribute levels. Then, convolutional neural network (CNN) backbones are developed with a dual objective of global serial correlation and local manifold regularization, which capture spatiotemporal information at both global and local scales, facilitating effective attribute encoding and characterization of flow states. Finally, the attribute evolution heat map and a monitoring metric (MM) collectively offer a compelling and comprehensive analysis of the three-phase flow process. Extensive experiments demonstrate that Ag-MRDCVA surpasses existing methods, showcasing its ability to minutely monitor the process while providing reasonable explanations.

## 1. Introduction

Oil-gas-water three-phase flow, a complex mixed flow of three immiscible media, is commonly encountered in petroleum and chemical industries. The flow process exhibits instability, nonlinearity, instantaneity and randomness, which pose great challenges to engineers and scholars. Monitoring the behavior and evolution of flow processes is imperative for promoting economic performance and ensuring operation safety (Gao & Jin, 2011).

In recent years, extensive efforts have been dedicated to exploring multiphase flow to obtain a wealth of process data and monitor the flow process. Various methods have been proposed for measuring phase holdup, including the ray method (Stahl & von Rohr, 2004), microwave method (Xu et al., 2023), ultrasonic method (Su et al., 2018), and electric method (Fossa, 1998). Additionally, for measuring flowrate and superficial velocities, cross-correlation method (Zhai et al., 2014), optical method (Ojima et al., 2014) and ultrasonic Doppler method (Shi

et al., 2022) have been developed. Since the 1980s, tomography has been extensively studied and applied to monitor multiphase flow due to their non-intrusive nature and image reconstruction capability (Fang et al., 2024; Liang et al., 2023). With the advancement of multi-sensor measurement technology, the abundant process data has paved the way for data-driven methods for analyzing and monitoring multiphase flow (AL-Qutami et al., 2018). OuYang et al. (2022) construct an ensemble model combining BiLSTM-CNN, attention mechanism and residual connection to conduct two-phase flow pattern identification and uncover flow dynamic behavior. Kuang et al. (2024) apply a weak-supervised learning-based two-phase flow regime identification solution using a nondestructive tests ultrasonic sensor by proposing a self-supervised feature extraction algorithm. However, most prevailing efforts concentrate on two-phase flows rather than three-phase flows.

\* Corresponding author.

E-mail addresses: [lilinghan@tju.edu.cn](mailto:lilinghan@tju.edu.cn) (L. Li), [fdong@tju.edu.cn](mailto:fdong@tju.edu.cn) (F. Dong), [shumeizhang@tju.edu.cn](mailto:shumeizhang@tju.edu.cn) (S. Zhang).

Besides, they emphasize flow pattern classification rather than comprehensive flow state monitoring and analysis, limiting their ability to continuously track the evolving three-phase flow state and provide deeper insights.

Nowadays, multivariate statistical analysis has emerged as a prominent research area in data mining and process monitoring (Yu et al., 2022), such as principal component analysis (PCA) (Wen & Xu, 2021) and partial least square (PLS) (Muradore & Fiorini, 2012). In most industrial processes, the involved data often exhibit strong dynamics and nonlinearity. It implies that the current sample is influenced by past samples, showing temporal correlation characteristics and complex data structures. In response to the task of process dynamics, methodologies such as slow feature analysis (SFA) (Puli et al., 2021) and canonical variate analysis (CVA) (Odiowei & Cao, 2010) are developed and successfully applied to monitor complex industrial processes. Specifically, CVA constructs a state-space model based on serially correlated data, aiming to maximize the correlation between past and future data in systems. Dong et al. (2021) utilize CVA to extract the state features of two-phase flow, subsequently inputting them into a Gaussian mixture model (GMM) for monitoring flow states. Ruiz-Carcel et al. (2015) verify the effectiveness of CVA on a multiphase flow experimental device, which evaluates the ability of CVA to detect faults in the actual system. To tackle the dual challenges of nonlinearity and dynamics, the combination of CVA and kernel method has been developed. For instance, Pilario et al. (2019) propose mixed kernel canonical variate dissimilarity analysis (MK-CVDA) for process incipient fault detection in nonlinear dynamic processes under varying operating conditions. Wang et al. (2022) propose kernel CVA (KCVA) for fault detection of a floating offshore wind turbine. Lou et al. (2023) propose modified mixed kernel-aided canonical stationary variate analysis (M2KCSVA) to address nonlinear and nonstationary problems in industrial process monitoring. Nevertheless, the kernel-based CVAs are nonparametric and their representation is limited by the fixed kernel.

Deep neural network (DNN) is another important approach in data-driven area, which has gained significant attention in process monitoring due to their abilities to capture complex nonlinearity and fit data, including convolutional neural network (CNN) (Nnabuife et al., 2021), autoencoder (Yang et al., 2024), recurrent neural network (RNN) (Peng et al., 2020), etc. In process control, leveraging information derived from the latest valid iterations alongside a continuously updated input sequence, which retains a history of valid input signals, proves advantageous, particularly for managing time-varying systems (Guan et al., 2023). Within the framework of system feedback, it becomes imperative for process monitoring to consider the serial correlation existing among current and past time samples, which can be captured through CVA. Additionally, the computational overhead required for traditional complex DNN renders it unsuitable for industrial environments where resource constraints are prevalent. Consequently, a burgeoning area of interest lies in the integration of DNN with CVA-based process monitoring methodologies (Yu et al., 2021) and developing lightweight networks. For instance, Chen et al. (2022) develop the stacked neural network-aided CVA for fault detection in nonlinear dynamic systems. Wu et al. (2021) combine deep CVA and Fisher discriminant analysis (DCVA-FDA), which constructs a residual generator from DCVA features. However, despite the effectiveness of DCVA in addressing process dynamics and nonlinearity, its applicability to the specific context of oil-gas-water three-phase flow might be constrained. This limitation arises from a lack of a close connection with the actual flow process, preventing a comprehensive analysis of the flow state.

The state monitoring of oil-gas-water three-phase flow requires a multi-faceted description, such as the dominant phase, the interphase structure between gas and liquid, and the interphase structure between oil and water (Açıkgoz et al., 1992). Such a description encompasses global and local information, which is difficult to obtain solely from labels or raw data. Moreover, due to the complexity of

the process and the limitations of safety requirements, the modeling efforts often encompass only a subset of the entire range of flow states. Therefore, it is crucial to effectively transfer the knowledge obtained from these modeled states to the entirety of the three-phase flow process. Deep transfer learning emerges as a viable solution to address this issue (Chen et al., 2024; Fallahdizcheh & Wang, 2022; Rezaee et al., 2023). In numerous transfer learning researches, semantic attributes play a pivotal role by providing supplementary information that facilitates comprehensive descriptions and analysis, which has also been used in zero-shot learning (ZSL) (Lampert et al., 2009), image recognition (Zhu et al., 2021) and preference prediction (Zhan et al., 2022). In process monitoring, attributes that describe structures and characteristics of the object are related to its state, which can be defined by expert knowledge and process mechanisms. Therefore, introducing semantic attributes and establishing a mapping between them and data are beneficial to mine the global-local information of processes and achieve knowledge transfer. However, to the authors' knowledge, the impact of attributes on process monitoring has not been extensively explored.

With the introduction of state attributes, combining interpretable attribute guidance with feature learning is an effective approach for constructing a monitoring model. To fully capture attribute-encoding features of three-phase flow processes, it is necessary to incorporate local spatiotemporal information with global serial correlation. However, classical CVA only captures the serial features of samples but ignores the local spatial structure. A recent work reveals that the event-triggered conditions and feature extraction of a network are tightly related to spatiotemporal distribution characteristic (Song et al., 2023). In the field of process monitoring, dynamic monitoring algorithms with manifold regularization have been verified to effectively extract the local geometric structure in dynamic processes (Li et al., 2023; Xu & Ding, 2021). Hence, the regularization for local manifold is introduced with reference to local preserving projection (LPP) (He & Niyogi, 2003), aiming to preserve the local structure during feature extraction as well as provide an accurate representation of the raw data and state attributes. Briefly speaking, we learn features within the CVA framework by injecting global and local spatiotemporal losses on intermediate layers of DNN, and enforce these features to encode different state attributes with attribute guidance. The interpretable state attributes and features cooperatively facilitate the monitoring results to be convincing and explainable.

In summary, there are several gaps which will be explored in this work: (1) The absence of a universally accepted definition and standardized flow regime maps for three-phase flow states poses challenges in categorizing them, necessitating a comprehensive flow state description. (2) The complexity of the three-phase flow process and numerous transition states underscore the importance of transferring knowledge from typical flow states to test states. (3) Owing to the nonlinearity and dynamics inherent in three-phase flow, conventional models fall short in extracting features that encode both global and local state attributes. Hence, an effective integration of local spatiotemporal information and global serial correlation within the deep learning framework is imperative.

Given the aforementioned considerations, this article proposes the manifold regularized deep canonical variate analysis with attribute guidance (Ag-MRDCVA) for three-phase flow process monitoring. Firstly, to enhance the richness of information, beyond merely labeling each flow state by categories, global and local state attributes are added as fine-grained auxiliary information, which comprehensively describe flow states and facilitate knowledge transfer from modeling states to testing states. Subsequently, the nonlinear transformations are learned through CNN backbones, with a focus on maximizing serial correlation and applying local manifold regularization. This design allows for the extraction of both global and local spatiotemporal information, which unveils intricate patterns and identifies anomalies and trends across various scales. Through the integration of attribute guidance, we

jointly optimize the attribute embedding and CNN for feature extraction, thereby encouraging high compatibility between the features and corresponding attribute vectors. Conclusively, the monitoring results are given by the attribute heat map and a monitoring metric (MM) combining features and attributes. The main contributions of this work are summarized as follows:

(1) Comprehensive and interpretable monitoring: This work provides a novel paradigm to monitor the oil–gas–water three-phase flow process, which introduces semantic attributes to describe multiphase flow. The attribute evolution heat map and MM corporately offer a convincing and comprehensive analysis of the flow process.

(2) State attribute-relevant feature extraction: An attribute guidance mechanism is designed to facilitate meaningful feature learning. It integrates attribute information as supervision at both the class and attribute levels, which compels the features to encode attribute information of flow process. Given the challenge of acquiring a substantial number of modeling samples for accurately modeling continuous transition processes, the well-designed attributes and extracted features play a pivotal role in transfer from modeling states to testing states.

(3) Global and local spatiotemporal information mining: The Ag-MRDCVA combines CVA and manifold learning to regularize the deep learning process, which aggregates both global and local spatiotemporal information, providing structure and physical meanings in the feature space. The dual-objective function of global serial correlation and local manifold structure in the network can take advantage of both CVA and LPP to extract meaningful information in nonlinear dynamic processes.

The remainder of this article is organized as follows: Section 2 provides the preliminaries of CVA and LPP. In Section 3, the methodology including problem statement, Ag-MRDCVA and a strategy of comprehensive state monitoring and analysis is proposed. Section 4 presents the experiments and results. Finally, Section 5 draws the conclusion and brings up future research expectation.

## 2. Preliminaries

### 2.1. Canonical variate analysis

CVA aims to maximize the correlations between the past and future sets of data. Assuming the observation vector  $\mathbf{x}_t$  at time  $t$  contains  $J$  variables, considering the temporal correlations,  $\mathbf{x}_t$  is expanded by  $p$  past and  $f$  future measurements to generate the past vector  $\mathbf{x}_{p,t}$  and future vector  $\mathbf{x}_{f,t}$

$$\mathbf{x}_{p,t} = [\mathbf{x}_{t-1}^T, \mathbf{x}_{t-2}^T, \dots, \mathbf{x}_{t-p}^T]^T \in \Re^{Jp} \quad (1)$$

$$\mathbf{x}_{f,t} = [\mathbf{x}_t^T, \mathbf{x}_{t+1}^T, \dots, \mathbf{x}_{t+f-1}^T]^T \in \Re^{Jf} \quad (2)$$

The determination of the optimal values for the past and future lags ( $p$  and  $f$ ) is elucidated in Odiouwei and Cao (2010). Then, the past matrix  $\mathbf{X}_p$  and future matrix  $\mathbf{X}_f$  are formed by appropriately arranging the past and future vectors, respectively

$$\mathbf{X}_p = [\mathbf{x}_{p,t+1}, \mathbf{x}_{p,t+2}, \dots, \mathbf{x}_{p,t+m}] \in \Re^{Jp \times m} \quad (3)$$

$$\mathbf{X}_f = [\mathbf{x}_{f,t+1}, \mathbf{x}_{f,t+2}, \dots, \mathbf{x}_{f,t+m}] \in \Re^{Jf \times m} \quad (4)$$

where  $m = n - f - p + 1$ ,  $n$  is the number of samples.

The covariance  $\Sigma_{pp}$ ,  $\Sigma_{fp}$  and cross-covariance  $\Sigma_{ff}$  of  $\mathbf{X}_p$  and  $\mathbf{X}_f$  can be calculated as

$$\Sigma_{pp} = \frac{1}{m-1} \mathbf{X}_p \mathbf{X}_p^T \in \Re^{Jp \times Jp} \quad (5)$$

$$\Sigma_{ff} = \frac{1}{m-1} \mathbf{X}_f \mathbf{X}_f^T \in \Re^{Jf \times Jf} \quad (6)$$

$$\Sigma_{fp} = \frac{1}{m-1} \mathbf{X}_f \mathbf{X}_p^T \in \Re^{Jf \times Jp} \quad (7)$$

The Hankel matrix is calculated by  $\Sigma_{pp}$ ,  $\Sigma_{fp}$  and  $\Sigma_{ff}$ . Subsequently, the singular value decomposition (SVD) is adopted as

$$\Sigma_{ff}^{-1/2} \Sigma_{fp} \Sigma_{pp}^{-1/2} = \mathbf{U} \Lambda \mathbf{V}^T \quad (8)$$

where  $\mathbf{U}$  and  $\mathbf{V}$  are orthogonal matrices consisting of singular vectors, and  $\Lambda$  is a diagonal matrix consisting of the nonnegative singular values in descending order.

Then, the transformation matrix  $\mathbf{J}$  can be derived as

$$\mathbf{J} = \mathbf{U}_r^T \Sigma_{pp}^{-1/2} \quad (9)$$

where  $\mathbf{U}_r$  contains the first  $r$  columns in  $\mathbf{U}$ .

Finally, the data are converted by  $\mathbf{J}$  to obtain a  $r$ -dimensional canonical variate (CV) matrix  $\mathbf{Z}$

$$\mathbf{Z} = \mathbf{J} \mathbf{X}_p \quad (10)$$

### 2.2. Locality preserving projections

LPP is a commonly-used manifold learning method, known for its ability to preserve the local geometric structure of the original data during dimension reduction (He & Niyogi, 2003). Given a data matrix  $\mathbf{x}$  with  $J$  variables and  $n$  samples, LPP determines the transformation matrix  $\mathbf{W}$  to minimize the difference between the pairwise distances of the original samples and their corresponding low-dimensional projections

$$\psi_{LPP} := \min_{\mathbf{W}} \sum_{i,j=1}^n (\mathbf{y}_i - \mathbf{y}_j)^2 H_{ij} \quad (11)$$

where  $\mathbf{y} = \mathbf{Wx}$  is the extracted feature;  $H_{ij}$  is the element in the proximity matrix  $\mathbf{H}$ ;  $H_{ij}$  represents the weight of the edge connecting vertices  $\mathbf{x}_i$  and  $\mathbf{x}_j$ , which can be computed using the heat kernel

$$H_{ij} = \begin{cases} \exp\left(-\|\mathbf{x}_i - \mathbf{x}_j\|^2 / \epsilon\right), & \text{if } \mathbf{x}_i, \mathbf{x}_j \in L(\mathbf{x}_i, \mathbf{x}_j) \\ 0, & \text{otherwise} \end{cases} \quad (12)$$

where  $\epsilon$  is a parameter for adjusting  $H_{ij}$ ;  $L(\mathbf{x}_i, \mathbf{x}_j)$  denotes the neighborhood.

Then, the objective function can be further derived as

$$\begin{aligned} \frac{1}{2} \sum_{i,j=1}^n (\mathbf{y}_i - \mathbf{y}_j)^2 H_{ij} &= \frac{1}{2} \sum_{i,j=1}^n (\mathbf{W}^T \mathbf{x}_i - \mathbf{W}^T \mathbf{x}_j)^2 H_{ij} \\ &= \sum_i \mathbf{W}^T \mathbf{x}_i D_{ii} \mathbf{x}_i^T \mathbf{W} - \sum_{ij} \mathbf{W}^T \mathbf{x}_i H_{ij} \mathbf{x}_i^T \mathbf{W} \\ &= \mathbf{W}^T \mathbf{x} (\mathbf{D} - \mathbf{H}) \mathbf{x}^T \mathbf{W} = \mathbf{W}^T \mathbf{x} \mathbf{L} \mathbf{x}^T \mathbf{W} \end{aligned} \quad (13)$$

where  $\mathbf{D}$  is a diagonal matrix in which  $D_{ii} = \sum_j H_{ji}$ ;  $\mathbf{L} = \mathbf{D} - \mathbf{H}$  is the Laplacian matrix.

The constraint is imposed as

$$\mathbf{W}^T \mathbf{x} \mathbf{D} \mathbf{x}^T \mathbf{W} = \mathbf{I} \quad (14)$$

The transformation  $\mathbf{W}$  can be derived by solving the generalized eigenvalue problem

$$\mathbf{L} \mathbf{W} \mathbf{x} = \lambda \mathbf{D} \mathbf{W} \mathbf{x} \quad (15)$$

## 3. Methodology

### 3.1. Problem statement

**Statement 1 :** In comparison to two-phase flows, the inclusion of a third phase introduces a higher complexity in flow states and phase distribution structures. Currently, there lacks a universally accepted definition for three-phase flow states, and a standardized three-phase flow regime map is yet to be established. Hence, labeling three-phase flow states by categories becomes challenging, emphasizing the necessity for a comprehensive description of flow states.

The prevailing method for describing oil–gas–water three-phase flow is the three-factor method (the dominant phase, the interphase

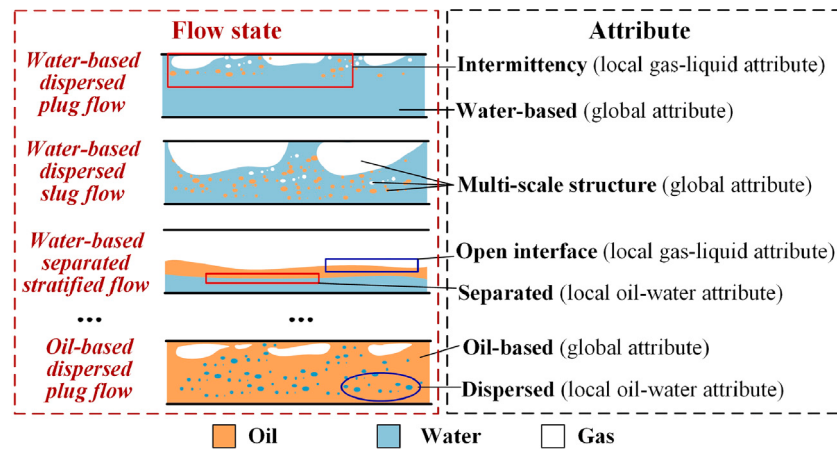


Fig. 1. Diagram of several attributes of three-phase flow.

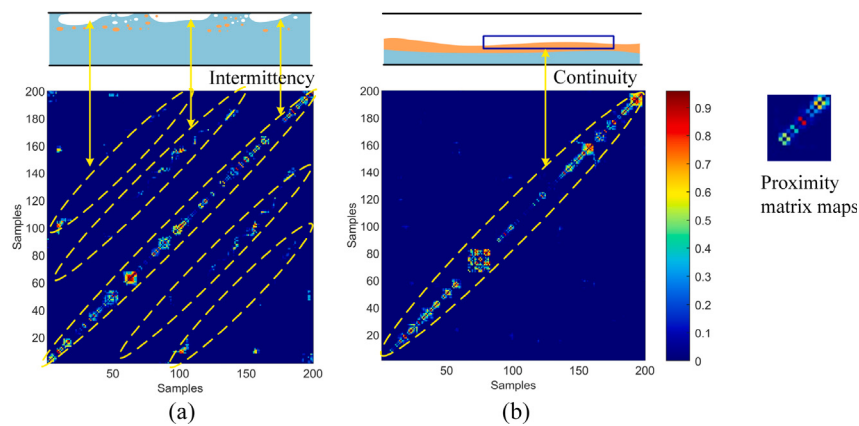


Fig. 2. Characterization for local attribute information by manifold structure. (a) shows the intermittency of flow states with bubble gas-liquid relation; (b) shows the continuity of flow states with stratified gas-liquid relation.

structure between gas and liquid, and the interphase structure between water and oil) (Açıkgoz et al., 1992). By defining appropriate state attributes associated with these factors, crucial global and local characteristics such as phase interactions, continuous phase behavior, and interface behavior between different phases can be captured. It facilitates a more precise and comprehensive depiction of flow state, as illustrated in Fig. 1. Moreover, multiphase flows usually involve numerous physical parameters, including flowrate, phase holdup, pressure, etc. By integrating flow parameters into state attributes, simpler and more intuitive analysis and modeling can be conducted. On this basis, interpretable attribute guidance is beneficial for feature extraction and modeling.

**Statement 2 :** State monitoring of oil–gas–water three-phase flow encompasses both global information (such as the dominant phase) and local information (such as the interphase structure). However, traditional models are inadequate for extracting features that encode both global and local state attributes.

For global information, the serial correlation of all variables along the time axis can reflect global attributes and state evolutions (Dong et al., 2021). For local information, different variables can extract various local behavior and dynamic evolution trends, since multimodal sensors have different pertinences for multiphase medium and flow characteristics. Such local correlations can be captured by convolution for variable blocks (Yu et al., 2021). Moreover, the manifold structure plays a pivotal role in encoding local attribute information. As shown in Fig. 2, the spatial manifold of consecutive samples from two distinct flow states is represented by the proximity matrix  $\mathbf{H}$ , where  $H_{ij}$  is larger for space-closer samples. In Fig. 2(a), the samples with large  $H$

are temporally distant from each other and present flow intermittency. In contrast, Fig. 2(b) shows a concentrated distribution of large  $H$  elements along the diagonal line, suggesting continuous fluctuations. Therefore, the spatial manifold structure serves as a regularization term for feature extraction, which cannot only extract local information, but also help to deal with high cross-correlation.

### 3.2. Proposed Ag-MRDCVA

The comprehensive framework of Ag-MRDCVA is illustrated in Fig. 3. The Ag-MRDCVA incorporates two CNN backbones for feature extraction. Besides, it includes an attribute guidance module, local manifold regularization, and global serial correlation extraction. The attribute prediction is accomplished by a shallow embedded network.

#### 3.2.1. Model input

The current sample vector is denoted as  $\mathbf{x}_t \in \mathbb{R}^J$ . Since the current sample and past data are available during online monitoring, in both modeling and monitoring, the past vector is extended from the current time  $t$  to the previous time. Furthermore, instead of being arranged as a vector like in (1), the past vectors are organized into a matrix denoted as  $\mathbf{x}_t^p$

$$\mathbf{x}_t^p = [\mathbf{x}_t, \mathbf{x}_{t-1}, \dots, \mathbf{x}_{t-p+1}]^T \in \mathbb{R}^{J \times p} \quad (16)$$

Correspondingly, the future data  $\mathbf{x}_t^f$  is constructed as

$$\mathbf{x}_t^f = [\mathbf{x}_{t+1}, \mathbf{x}_{t+2}, \dots, \mathbf{x}_{t+f}]^T \in \mathbb{R}^{J \times f} \quad (17)$$

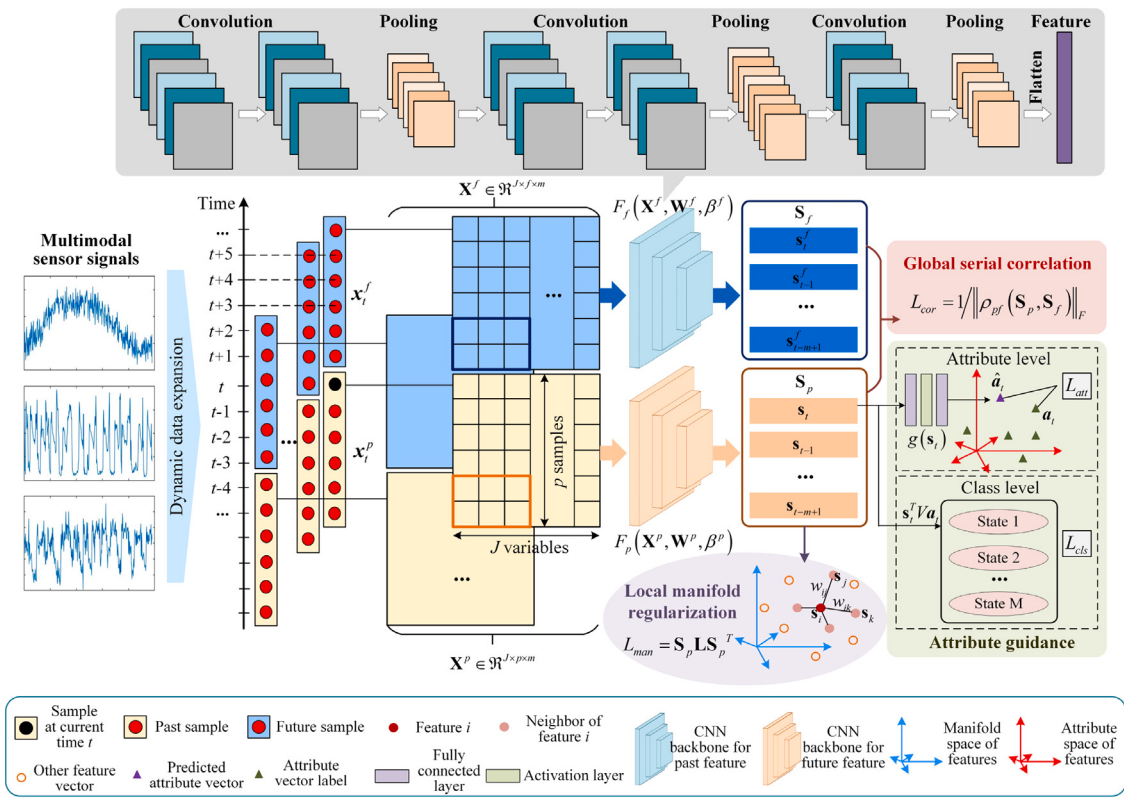


Fig. 3. Overview of the proposed Ag-MRDCVA framework.

Then, the data are normalized to avoid domination of those variables with higher absolute values measured

$$\hat{x}_t^p = x_t^p - \bar{x}_t^p \quad (18)$$

$$\hat{x}_t^f = x_t^f - \bar{x}_t^f \quad (19)$$

where  $\bar{x}_t^p$  and  $\bar{x}_t^f$  are the sample means of  $x_t^p$  and  $x_t^f$ , respectively.

$x_t^p$  and  $x_t^f$  can be treated as 2D data matrices, which align with online monitoring and are tractable for CNN. In Ag-MRDCVA, the traditional CVA's past and future matrices are generalized to the past and future matrix sets

$$\mathbf{X}^p = \left\{ x_i^p, x_{i-1}^p, \dots, x_{i-m+1}^p \right\} \in \mathbb{R}^{J \times p \times m} \quad (20)$$

$$\mathbf{X}^f = \left\{ x_i^f, x_{i-1}^f, \dots, x_{i-m+1}^f \right\} \in \mathbb{R}^{J \times f \times m} \quad (21)$$

where  $m = n - f - p + 1$ ,  $n$  is the number of all samples.

### 3.2.2. Base CNN module for feature extraction

The CNN backbones serve as the primary feature extractors, which are capable of efficiently processing the sequential 2D data matrices and extracting local correlations from different variable blocks. Formally, the variable-sample unit at position  $(j, k)$  in the  $i$ th feature map of the  $l$ th layer with activation function  $\sigma$  is presented as

$$c_{l,i}^{j,k} = \sigma \left( \sum_{w=0}^{K_W-1} \sum_{h=0}^{K_H-1} w_{l,i}^{w,h} c_{i-1}^{(j+w)(k+h)} + b_{l,i} \right) \quad (22)$$

where  $w_{l,i}^{w,h}$  is the value of the  $i$ th kernel at the position  $(w, h)$  with the size of  $K_W$ ,  $K_H$  in the  $l$ th layer, respectively;  $b_{l,i}$  is the bias.

The maximum pooling operation is used to combine adjacent features into one element

$$c^p(j, k) = \max \left\{ c_{l,i}^{j',k'} \mid j' \leq j \leq j + K_W - 1, k' \leq k \leq k + K_H - 1 \right\} \quad (23)$$

Each CNN model of the Ag-MRDCVA is connected as: two convolution layers - one pooling layer - two convolution layers - one pooling layer - one convolution layer - one pooling layer, as shown in Fig. 3. Finally, two separated CNNs transform the past and future data to the features

$$s_t^p = f_p(x_t^p, W^p, \beta^p) \in \mathbb{R}^r \quad (24)$$

$$s_t^f = f_f(x_t^f, W^f, \beta^f) \in \mathbb{R}^r \quad (25)$$

where  $s_t^p$  and  $s_t^f$  are the extracted features, and  $s_t = s_t^p$  is the preserved CV set;  $r$  is the retained feature dimension;  $f_p(\cdot, W^p, \beta^p)$  and  $f_f(\cdot, W^f, \beta^f)$  are the feature mapping functions, and  $f(\cdot, W, \beta) = f_p(\cdot, W^p, \beta^p)$  is preserved, because only the current and past data are available during online application;  $W^p$  and  $W^f$  refer to the network weights;  $\beta^p$  and  $\beta^f$  denote the network biases.

### 3.2.3. Global serial correlation extraction

In the three-phase flow process that is inherently dynamic, a notable correlation exists between past and future data. To effectively capture the evolution of the flow state and characterize its global attributes, it is necessary to maximize the cross-correlation between past features  $S_p = [s_t^p, s_{t-1}^p, \dots, s_{t-m+1}^p] \in \mathbb{R}^{r \times m}$  and future features  $S_f = [s_t^f, s_{t-1}^f, \dots, s_{t-m+1}^f] \in \mathbb{R}^{r \times m}$

$$\max \rho_{pf}(S_p, S_f) = \max \frac{\text{cov}(S_p, S_f)}{\sqrt{\text{var}(S_p)} \sqrt{\text{var}(S_f)}} \quad (26)$$

$$L_{cor} = 1 / \|\rho_{pf}[F_p(\mathbf{X}^p, W^p, \beta^p), F_f(\mathbf{X}^f, W^f, \beta^f)]\|_F \quad (27)$$

where  $\rho_{pf}$  is the Pearson's correlation coefficient;  $F_p(\cdot, W^p, \beta^p)$  indicates the utilization of  $f_p(\cdot, W^p, \beta^p)$  to extract features from the past dataset  $\mathbf{X}^p$ , and  $F_f(\cdot, W^f, \beta^f)$  signifies the same operation.

### 3.2.4. Local manifold regularization

The sample space of three-phase flow state possesses a manifold structure that encapsulates local attribute information. In order to maintain the original manifold structure, it is essential to introduce manifold regularization into the feature embedding. Hence, the nearest neighbor of each sample is constructed in the original space  $\mathbf{X}^p$  using K-nearest neighbor (KNN) method, as described in (12). Then, in the feature space where the new embeddings are constructed, the optimization objective in (13) is modified as

$$\min \mathbf{S}_p \mathbf{L} \mathbf{S}_p^T \quad (28)$$

$$L_{man} = F_p(\mathbf{X}^p, \mathbf{W}^p, \beta^p) \mathbf{L} F_p(\mathbf{X}^p, \mathbf{W}^p, \beta^f)^T \quad (29)$$

### 3.2.5. Attribute embedding and attribute guidance

The class logits considers both features and attributes, providing a mechanism for adjusting feature extraction guided by attributes. Specifically, the extracted features are mapped to the class embedding space, and the class logits  $z$  is generated by computing the dot product between these features and attribute vectors

$$z = \mathbf{s}_t^T V \cdot \mathbf{a}_t \quad (30)$$

where  $V$  is a linear mapping;  $\mathbf{a}_t$  is the attribute label vector.

Cross entropy loss is calculated to encourage features to have high compatibility with their assigned attribute vectors at class level and suppress undesirable attribute co-occurrence

$$L_{cls} = -\log \left[ \exp(z) / \sum_{y_j \in Y} \exp(z_j) \right] \quad (31)$$

Additionally, the attribute prediction task is treated as a regression problem  $\hat{\mathbf{a}}_t = g(\mathbf{s}_t)$ , which is implemented by a shallow embedded network consisting of fully connected layers and a ReLU activation layer. The mean square error (MSE) between the predicted attribute vector and the ground truth attribute vector is minimized, enhancing the ability of the features to represent the state information at attribute level

$$L_{att} = \|\hat{\mathbf{a}}_t - \mathbf{a}_t\|_2^2 = \|g(\mathbf{s}_t) - \mathbf{a}_t\|_2^2 \quad (32)$$

### 3.2.6. Joint learning with attribute guidance

The joint training enhances the extraction of both global and local attribute information, facilitating the acquisition of comprehensive flow knowledge and accurate characterization of three-phase flow states. Both spatial structure and temporal correlation can be preserved, which inherits the advantage of CVA in handling high-dimensional data with serial correlation and the strength of manifold learning in pattern recognition. To achieve this, the objectives are simultaneously optimized

$$L_{all} = L_{cor} + \lambda_{man} L_{man} + \lambda_{cls} L_{cls} + \lambda_{att} L_{att} + \lambda_I \|\mathbf{s}_t \mathbf{s}_t^T - \mathbf{I}\| \quad (33)$$

where  $\lambda_{man}$ ,  $\lambda_{cls}$ ,  $\lambda_{att}$  and  $\lambda_I$  are the hyper-parameters. It is noteworthy that the inclusion of the last term in the objective function serves to prevent trivial solutions.

To summarize, the pseudocode of Ag-MRDCVA is listed in **Algorithm 1**.

### 3.3. Comprehensive state monitoring and analysis

For monitoring the state of the oil-gas-water three-phase flow process, a shallow embedded network is employed to predict the attribute vector  $\hat{\mathbf{a}}_t = g(\mathbf{s}_t)$ . Unlike binary values, the attribute vector comprises continuous values, providing a more accurate description of the evolution process, particularly during transitional stages. Besides, the predicted attribute matrix offers expert knowledge and sufficient decision-making information for the flow process rather than a simple identification of flow states.

### Algorithm 1 Ag-MRDCVA

---

```

1: Input: Past matrix set  $\mathbf{X}^p \in \mathbb{R}^{J \times p \times m}$ , future matrix set  $\mathbf{X}^f \in \mathbb{R}^{J \times f \times m}$ , attribute label  $A$ , and class label  $Y$ .
2: Hyper-parameters: Time-lags  $p$  and  $f$ ;  $\epsilon$  for adjusting the proximity matrix; the size of the convolution kernel for each layer  $K_W \times K_H$ ; regularization parameters  $\lambda_{man}$ ,  $\lambda_{cls}$ ,  $\lambda_{att}$  and  $\lambda_I$ ; learning rate  $\alpha$ , momentum, minibatch size, and maximum number of epoch  $N_{me}$ .
3: Output: Feature embedding function  $f(\cdot, \mathbf{W}, \beta)$ , attribute embedding function  $g(\cdot)$ .
4: Initialize CNN filters  $\mathbf{W}^p$  and  $\mathbf{W}^f$ , and biases  $\beta^p$  and  $\beta^f$ , attribute embedding function  $g(\cdot)$ .
5: for  $e = 1$  to  $N_{me}$  do
6:   for each mini-batch in  $\mathbf{X}^p$  and  $\mathbf{X}^f$  do
7:      $X_{batch,p}, A_{batch,p}, Y_{batch,p} \leftarrow$  samples from  $\mathbf{X}^p$ , attribute labels from  $A$ , and class labels from  $Y$ 
8:      $X_{batch,f} \leftarrow$  samples from  $\mathbf{X}^f$ 
9:     Forward Pass:
10:    Compute features  $s_p = f_p(X_{batch,p}, W^p, \beta^p)$ , and  $s_f = f_f(X_{batch,f}, W^f, \beta^f)$ 
11:    Predict attributes  $\hat{a} = g(s_p)$ 
12:    Compute class logits  $z_p = s_p^T V \cdot A_{batch,p}$ 
13:    Compute loss  $L_{cor}$ ,  $L_{man}$ ,  $L_{cls}$ ,  $L_{att}$  by (27)-(32)
14:    Compute total loss function  $L_{all}$  by (33)
15:    Backward Pass:
16:      Compute gradients  $\nabla_{W^p}, \nabla_{\beta^p}$  =
        Backprop( $X_{batch,p}, A_{batch,p}, Y_{batch,p}$ )
17:      Update parameters:  $W^p = W^p - \alpha \nabla_{W^p}$ ,  $\beta^p = \beta^p - \alpha \nabla_{\beta^p}$ 
18:      Update attribute embedding:  $g(\cdot) \leftarrow g(\cdot)^+$ 
19:       $f(\cdot, W, \beta) \leftarrow f_p(\cdot, W^p, \beta^p)$ 
20:    end for
21: end for

```

---

While class logits  $z$  in (30) can intuitively identify typical three-phase flow states involved in modeling, relying solely on the criterion of selecting the largest class logits for determining the flow state may result in misclassifying transition states as typical flow states. Actually, the attributes and features of typical flow states have high compatibility, resulting in a high maximum class logits value. However, because the training data are all from typical flow states, the attributes are more difficult to match with the features of transition states during test, leading to a low maximum class logits value. To address this issue, the monitoring metric (MM) denoted by  $\mathcal{M}$  is computed as

$$\mathcal{M} = \max(\mathbf{s}_t^T V \cdot \mathbf{a}_y) \quad (34)$$

where  $\mathbf{a}_y$  is the attribute vector of class  $y$ .

During modeling, the low control limit (LCL) for MMs of all the typical flow states is calculated by kernel density estimation (KDE) method (Odiwei & Cao, 2010), which can distinguish between typical flow states and transition states

$$\alpha_u = \int_{-\infty}^{LCL} p(\mathcal{M}) dz \quad (35)$$

where  $\alpha_u$  is the suitable confidence level;  $p(\mathcal{M})$  is the probability density function (PDF) of  $\mathcal{M}$ , which can be estimated through a kernel function  $K$

$$\hat{p}(z) = \frac{1}{nh} \sum_{k=1}^n K \left( \frac{\mathcal{M} - \mathcal{M}_k}{h} \right) \quad (36)$$

During online monitoring, the flow state is classified as a typical flow state if its MM reaches LCL. Conversely, if MM is lower than LCL, it indicates that the flow process is in transition. Mathematically, the criterion for identifying typical flow states is defined as

$$\hat{y} = \arg \max_{y \in Y} \mathbf{s}_t^T V \cdot \mathbf{a}_y, \text{ and } \mathcal{M} > LCL \quad (37)$$

**Table 1**  
Hyperparameters in Ag-MRDCVA model.

Parameter	Description	Suggested range
$p$	length of past observations	[15, 30]
$f$	length of future observations	[15, 30]
$\epsilon$	bandwidth of neighborhood weights	(0, 2)
$K_W \times K_H$	size of convolution kernel	[3 × 2, 7 × 7]
$\lambda_{man}$	regularization of local manifold structure	(0, 1]
$\lambda_{cls}$	regularization of class supervision	(0, 1]
$\lambda_{att}$	regularization of attribute supervision	(0, 1]
$\lambda_I$	regularization of unit variance	(0, 1]

### 3.4. Analysis and discussion

#### 3.4.1. Parameter setting

In Ag-MRDCVA, several parameters should be predefined, including the number of time-lags  $p$  and  $f$  for the extraction of global temporal correlation,  $\epsilon$  for adjusting the proximity matrix, the size of the convolution kernel for each layer  $K_W \times K_H$ , and the regularization parameters to balance the impact of each term in the objective function  $\lambda_{man}$ ,  $\lambda_{cls}$ ,  $\lambda_{att}$  and  $\lambda_I$ .

The length of the past and future observations  $p$  and  $f$  can be determined by checking the autocorrelation of the square sum of the process variables (Odiowei & Cao, 2010). The bandwidth parameter  $\epsilon$  controls the decay rate of kernel function and affects the distribution of neighborhood weights, which is selected by cross-validation in this work. The configuration of  $K_W \times K_H$  can be referred to Yu et al. (2021), which depends on the sampling rate and the order of the process system and the number of variables.  $\lambda_{man}$  controls the relative influence between global temporal correlation and local manifold structure.  $\lambda_{cls}$  and  $\lambda_{att}$  mainly adjust the relative influence between supervisions at class level and attribute level. They can be adjusted through cross-validation.  $\lambda_I$  prevents trivial solutions, which is set to a fixed value of 0.1 in this work. Table 1 lists these hyperparameters to be determined.

#### 3.4.2. Theoretical analysis

In the loss function (33), cross-correlations among features are computed to capture temporal dependencies, ensuring the representation of global temporal correlations between past and future features. The extraction for dynamic natures is beneficial for encoding global attributes. Furthermore, the Ag-MRDCVA involves calculating the similarity between samples using the RBF and constructing an adjacency matrix based on this similarity measure, then the Laplacian matrix  $L$  is computed to capture the local manifold structure within the data. The regularization of spatial manifold structure cannot only extract local information, but also help to deal with high cross-correlation. Moreover, incorporating attribute and class errors into the loss function offers supervision at both the attribute and class levels, thereby enhancing the model's overall performance and interpretability.

For effectively training Ag-MRDCVA, two CNN backbones with the same structure and one shallow attribute predictor need to be optimized. Each CNN backbone consists of 5 convolutional layers and 3 pooling layers. ReLU activation functions are utilized in the CNN backbones to facilitate the learning of nonlinear relationships. Additionally, the sparse activation properties of ReLU can mitigate the vanishing gradient problem, leading to faster network training. The output is one-dimensional feature vectors, serving as the basis for subsequent attribute prediction and classification tasks. Thus, the CNN backbone for  $X^p$  acts as the feature extractor. In the shallow attribute predictor, the extracted features are mapped to a vector space with 11 attributes (11 attributes are defined to describe three-phase flow states in this work) through a fully connected layer.

## 4. Experiments and results

### 4.1. Experiment description

#### 4.1.1. Dynamic experiment of multiphase flow and data acquisition

The oil-gas-water three-phase flow experiment is conducted on the multiphase flow experimental facility at Tianjin University. The stainless-steel horizontal pipe has an inner diameter of 50 mm and a total length of 16 m. To regulate and measure the flowrate of each phase, regulator valves and standard single-phase flowmeters with an accuracy of 0.5% are installed in each single-phase pipeline. Various flow states can be generated by manipulating the flowrate of each phase. In this experimental setup, the fluid comprises tap water (density 998 kg/m<sup>3</sup>, dynamic viscosity  $1.01 \times 10^{-3}$  Pa s), industrial mineral oil (density 790 kg/m<sup>3</sup>, dynamic viscosity  $3.9 \times 10^{-2}$  Pa s) and dry air (density 1.2 kg/m<sup>3</sup>, dynamic viscosity  $1.81 \times 10^{-5}$  Pa s).

To make the flow state fully developed, the test section is located approximately 13 m downstream from the inlet, where the pulse-wave ultrasonic Doppler (PWUD) sensor (Shi et al., 2021), continuous-wave ultrasonic Doppler (CWUD) sensor (Shi et al., 2022) and capacitance-conductance sensor (Shi et al., 2021) are installed. The PWUD sensor focuses on fluctuations at gas-liquid interface, the CWUD sensor pays attention to phase velocities, and the capacitance-conductance sensor provides information on water holdup. Additionally, a digital camera is utilized to record real-time flow states. The depictions of the experimental setup, including the test loop and combined multimodal sensor, are presented in Fig. 4. Ten typical flow states are formed in the experiment, and their photos are shown in Fig. 5. Details of the experiment points are listed in Table 2.

#### 4.1.2. State attribute definition

In this study, 11 fine-grained state attributes are defined for describing different flow states of three-phase flow, as detailed in Table 3. These attributes are critical descriptors capturing the flow characteristics of different flow states. Correspondingly, the state attribute matrix  $A$  is presented in Fig. 6, where the attribute values range from 0 to 5 levels and they are normalized during state monitoring. The multiple-level value indicates the degree of an attribute or the position of a fluctuation attribute. This approach enhances the precision of state descriptions, enabling a more refined analysis and continuous monitoring of the dynamic and evolving processes of the three-phase flow.

#### 4.1.3. Implementation

The Ag-MRDCVA network is trained on PyTorch. The architecture is completed on a computer with Intel(R) i7-9750H CPU and NVIDIA GeForce GTX 1660Ti GPU and 32 GB memory. The Adam optimizer (Kingma & Ba, 2014) is used with  $\beta_1 = 0.9$  and  $\beta_2 = 0.999$ . The learning rate is set as 0.01, and 300 epochs are conducted with batch size 64. The number of time-lags  $p$  and  $f$  are determined as 20 through autocorrelation analysis. The bandwidth parameter  $\epsilon$  is set as 1 by cross-validation. The proposed method is lightweight with minimal hardware configuration requirements. It is easy to deploy in hardware and embedded systems in practical industries.

#### 4.1.4. Evaluation indicators

In this work, 200 samples are used for testing within each typical flow state. Since the data set is balanced, accuracy has been chosen as the performance evaluation indicator. For each typical three-phase flow states, the accuracy is defined as

$$\text{Accuracy}_{num} = \frac{TP_{num} + TN_{num}}{TP_{num} + FP_{num} + TN_{num} + FN_{num}} \quad (38)$$

where  $TP_{num}$  is the true positives,  $FP_{num}$  is the false positives,  $TN_{num}$  is the true negatives, and  $FN_{num}$  is the false negatives of the  $num$ th flow state.

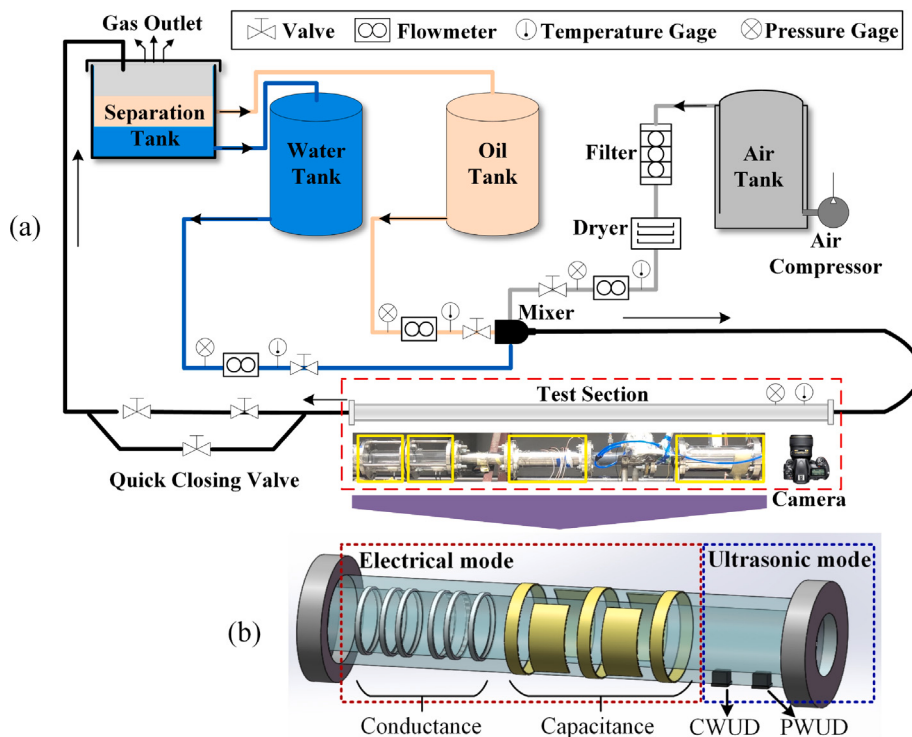


Fig. 4. Multiphase flow experiment device. (a) Test loop, (b) Schematic of multiple sensors.

**Table 2**  
Typical flow states and experiment conditions.

State	Dominant phase	Oil–water relation	Gas–liquid relation	Oil flowrate (m <sup>3</sup> /h)	Water flowrate (m <sup>3</sup> /h)	Gas flowrate (m <sup>3</sup> /h)
1	Water	Dispersed	Bubble	1.17–3.14	5.00	0.36–0.41
2	Water	Dispersed	Plug	1.17–3.00	5.00	1.27–4.74
3	Water	Dispersed	Slug	1.15–2.96	5.00	5.88–44.98
4	Water	Dispersed	Wave	0.60	0.60–0.90	42.43–90.00
5	Water	Separated	Stratified	0.60	0.60–2.05	1.26–2.30
6	Water	Dispersed	Annular	0.92–2.90	5.00	57.05–68.63
7	Oil	Dispersed	Bubble	5.00	0.51–1.07	0.30–0.42
8	Oil	Dispersed	Plug	5.00	0.58–1.15	1.27–4.73
9	Oil	Dispersed	Slug	5.00	0.47–1.19	5.87–42.39
10	Oil	Dispersed	Annular	5.00	0.49–1.03	102.69–106.34

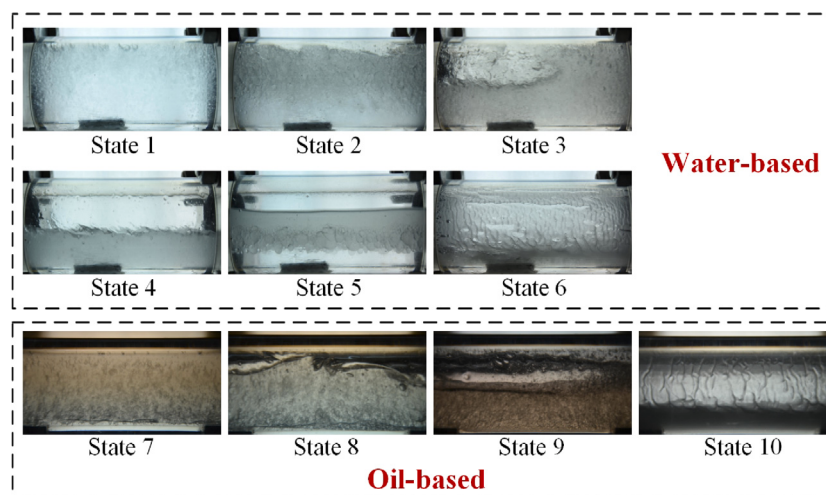


Fig. 5. Photos of typical oil–gas–water three-phase flow states.

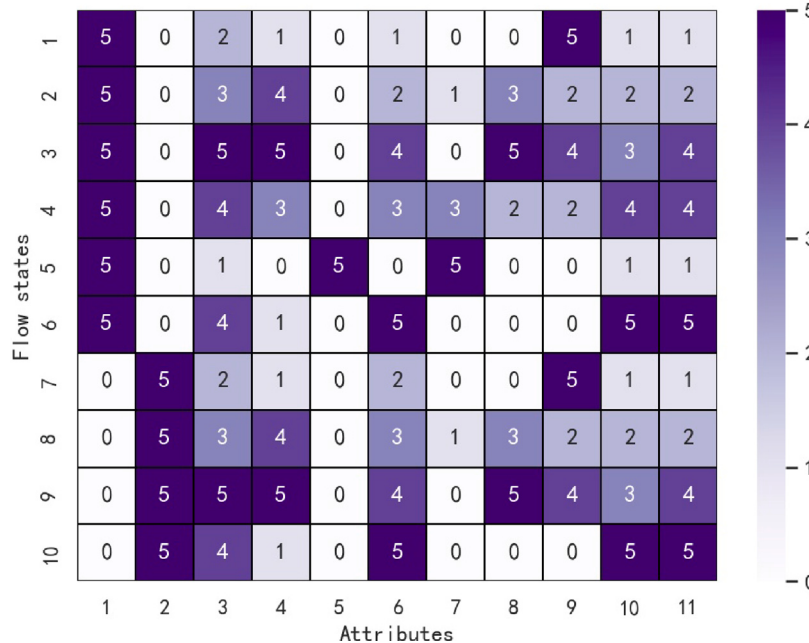


Fig. 6. State attribute matrix for typical three-phase flow states.

**Table 3**  
Attributes for oil-gas-water three-phase flow.

No.	State attributes	Attribute type
1	Water-based	Global attribute
2	Oil-based	Global attribute
3	Fluctuation degree	Global attribute
4	Multi-scale flow structure	Global attribute
5	Separation degree between liquid phases	Local oil-water attribute
6	Dispersion of non-dominant liquid phase	Local oil-water attribute
7	Opening degree of gas-liquid interface	Local gas-liquid attribute
8	Intermittency	Local gas-liquid attribute
9	Number of bubbles	Local gas-liquid attribute
10	Position of gas-liquid interface	Local gas-liquid attribute
11	Flow velocity of gas phase	Local parameter attribute

This metric reflects the proportion of all samples correctly classified by the model, which is preferred for its intuitive interpretation and broad applicability. Furthermore, the average accuracy for all the typical three-phase flow states is defined as

$$\text{Accuracy}_{\text{all}} = \frac{1}{N} \sum_{\text{num}=1}^N \text{Accuracy}_{\text{num}} \quad (39)$$

where  $N$  is the total number of typical three-phase flow states in the experiment.

#### 4.2. Identification for typical flow states

The comparative experiment is conducted to assess the performance of the proposed Ag-MRDCVA model. To conduct a thorough comparative study, several commonly-used methods are employed for feature extraction, including deep SFA (Chiplunkar & Huang, 2021), fully connected neural network (FCNN), RNN (Peng et al., 2020), CNN (Nnabuife et al., 2021), and KCVA (Wang et al., 2022).

##### 4.2.1. Parameter configurations for different modules

Various parameter configurations are established first to analyze their impacts within the Ag-MRDCVA framework. We mainly focus on assessing the influence of global and local spatiotemporal information, as well as supervisions at both the class and attribute levels, on feature extraction and identification performance. Therefore,  $\lambda_{\text{man}}$

**Table 4**  
Identification performance of Ag-MRDCVA with different parameter configurations.

No.	$\lambda_{\text{man}}$	$\lambda_{\text{cls}}$	$\lambda_{\text{att}}$	$\lambda_I$	Accuracy
1	0.3	0.2	0.05	0.1	89.00%
2	0.3	0.2	0.1	0.1	87.35%
3	0.3	0.2	0.2	0.1	85.65%
4	0.6	0.2	0.05	0.1	91.00%
5	0.6	0.2	0.1	0.1	91.30%
6	0.6	0.2	0.2	0.1	90.55%
7	1.0	0.2	0.05	0.1	90.35%
8	1.0	0.2	0.1	0.1	89.40%
9	1.0	0.2	0.2	0.1	89.00%

is set from 0.3 to 1 on validation datasets.  $\lambda_{\text{cls}}$  is set as 0.2, and  $\lambda_{\text{att}}$  is set as ranges from 0.05 to 0.2.  $\lambda_I$  is set as 0.1. The identification performance of Ag-MRDCVA with different parameters for ten typical three-phase flow states is summarized in Table 4. As shown in this table, with  $\lambda_{\text{att}}$  unchanged, the model's performance demonstrates an initial improvement followed by a subsequent decline as the parameter  $\lambda_{\text{man}}$  increases, which suggests the necessity for achieving a balanced configuration between global and local spatiotemporal information during feature extraction. Moreover, an appropriate  $\lambda_{\text{att}}$  can enhance model performance, but excessively small  $\lambda_{\text{att}}$  may lead to challenges in generalization. This is particularly evident due to the difficulty in attribute transfer from typical states to testing states. Hence, the 5th group parameter setting is selected to not only achieve high recognition accuracy for typical flow patterns but also enhance the model's ability to transfer attribute knowledge.

##### 4.2.2. Model performance

After analyzing the parameter configurations and effects, the well-designed Ag-MRDCVA architecture is evaluated. Fig. 7 presents the identification result for ten typical flow states. The left axis provides labels for the data corresponding to each state category, while the legend on the right indicates the color representing the class of data. The typical flow states can be accurately identified with high temporal resolution. However, certain flow state categories show lower accuracies, such as 68% for state 3. This is primarily due to the complexity of the flow process. State 2 and state 3 have the same continuous phase and interphase structure between water and oil, differing only in the

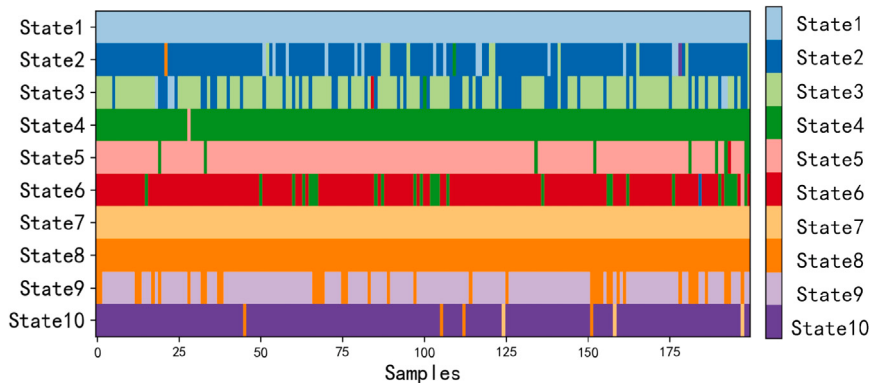


Fig. 7. Identification results for typical states of the three-phase flow process.

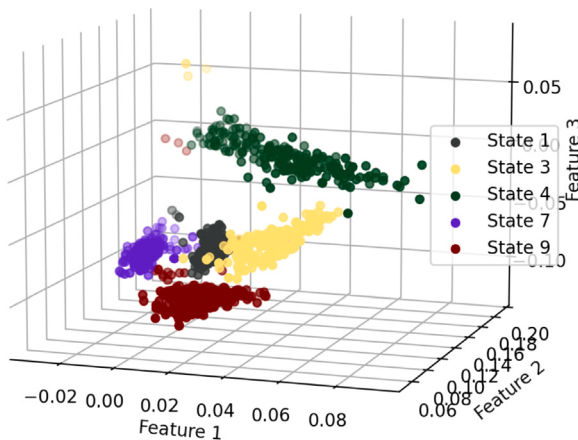


Fig. 8. Projection results in feature subspaces of test samples.

interphase structure between gas and liquid. Moreover, the gas–liquid structures of plug and slug share many similar characteristics, such as intermittency and a closed gas–liquid interface.

To further illustrate the discernibility of Ag-MRDCVA, test samples of five typical flow states are projected into subspaces created by the features, as depicted in Fig. 8. It is evident from the figure that the samples from each flow state are clearly separated in the discriminant subspace, with the projections of the flow states being far away from the centers of the others.

#### 4.2.3. Comparison results

The comparison results are summarized in Table 5. As anticipated, Ag-MRDCVA attains the highest identification accuracy, reaching 91.30% for typical three-phase flow states. This can be attributed to its ability to uncover more information on nonlinear dynamics, as well as global and local attributes. A more in-depth understanding of the identification performance is available in the confusion matrices of the test results with each model, depicted in Fig. 9. The rows represent the actual classes and its columns represent the predicted classes. From the confusion matrices, various metrics like accuracy, precision, recall, and F1 score can be calculated to evaluate the performance of the model. Notably, in this section, the test data is only roughly identified as some typical flow states. However, three-phase flow processes should be continuously and comprehensively monitored, which will be presented in detail in Section 4.3.

#### 4.2.4. Ablation study

An ablation study is conducted to evaluate the impact and highlight the significant contributions of each component in the proposed Ag-MRDCVA model. The study compares the performance of different

**Table 5**  
Identification accuracy of different methods.

Method	Testing accuracy
Ag-MRDCVA	91.30%
Deep SFA	87.15%
FCNN	87.65%
RNN	89.30%
KCVA	85.35%
CNN	88.35%

**Table 6**  
Ablation study of Ag-MRDCVA.

Method	$L_{cor}$	$L_{man}$	$L_{cls}$	$L_{att}$	Testing accuracy
Base DCVA	✓				86.20%
$+L_{man}$	✓	✓			88.05%
$+L_{cls}$	✓	✓	✓		89.75%
$+L_{att}$	✓	✓	✓	✓	91.30%

variants by adding the manifold regularization  $L_{man}$ , the attribute guidance at class level  $L_{cls}$ , and the attribute guidance at attribute level  $L_{att}$  gradually. The baseline is a base CNN module with serial correlation loss, referred to as base DCVA.

The results of the ablation study are presented in Table 6. It demonstrates the consecutive improvement in identification performance achieved by the full Ag-MRDCVA model over the base DCVA model, with an increase of 5.10%. The addition of the manifold regularization component prompts the model to extract local spatial information from the flow process, resulting in a performance boost of 1.85%. This finding suggests that incorporating spatial locality into the state representation enables the model to learn more discriminative features, leading to a significant improvement in state characterization and identification. Furthermore, the attribute guidance at the class level, which aims to suppress unwanted attribute co-occurrence and encourage features to align with their assigned attribute vectors in classes, provides an additional accuracy gain of 1.70%. This component helps ensure that the learned features are more compatible with the desired attribute representations, further enhancing the learning ability for attribute knowledge of flow process. Lastly, the attribute regression loss at the attribute level plays a crucial role in supervising the learning of each attribute and enforcing the features to capture both global and local attribute information. This component contributes to a performance boost of 1.55%.

#### 4.2.5. Complexity analysis

In contrast to pursuing SOTA without considering computational cost, the objective is to craft efficient networks so that CVA-based process monitoring techniques can be extended to the framework of deep learning and combined with manifold regularization. Moreover, our emphasis lies on advancing and validating a novel monitoring

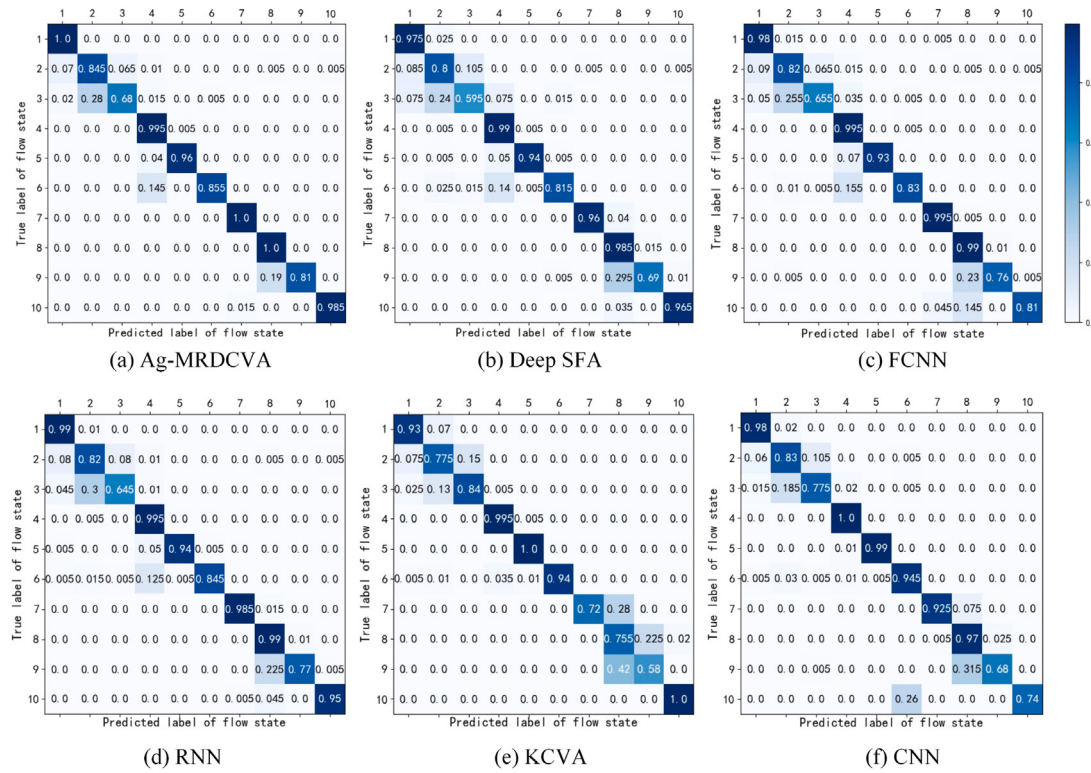


Fig. 9. Confusion matrices of test results using different methods.

paradigm for multiphase flow processes, using attribute transfer and attribute evolution heat maps. For the complexity analysis of Ag-MRDCVA, its floating-point operations (FLOPs), model parameters, and inference time are calculated. With Ag-MRDCVA comprising two CNN backbones and a shallow attribute predictor, we find the FLOPs to be 13.74 M, model parameters totaling 0.29 M, and an inference time of 0.54 ms. It can be found that the proposed method requires less computing power and is conducive to practical application.

#### 4.3. Monitoring and analysis for transition processes

The complexity of the evolution of oil–gas–water three-phase flow necessitates a comprehensive analysis of the transition process. Different from traditional process monitoring strategies reliant on multiple statistics, this study introduces an innovative paradigm utilizing state attributes for process description and analysis. This approach not only offers a more nuanced understanding of the system dynamics but also provides guidance for determining the direction of evolution, thereby facilitating effective process control. Three specific transition processes are studied as an emphasis: Case #1 transition from state 1 to state 3, Case #2 transition from state 7 to state 9, and Case #3 transition from state 5 to state 4.

Fig. 10(a) shows the monitoring results for Case #1, with a specific focus on the detailed analysis of state attributes. The flow process is effectively visualized and elucidated through a heatmap presenting the evolution of attributes. Key observations from the analysis are detailed below: Attributes A1 and A2 uniformly describe the dominant phase as water during the whole transition process. A3 illustrates a progressive intensification of fluctuations, indicating dynamic changes within the system. A4 increases continuously, highlighting the coexistence of complex multiscale structures such as gas slugs, bubbles, and oil droplets. A5 and A6 demonstrate that the structure between oil and water remains dispersed throughout the flow process. Additionally, with an increase in gas flow rate, the size of oil droplets in water decreases, enhancing dispersion. A7 consistently remains at a low

level, indicating that the gas–liquid interface is closed. A8 exhibits a progressive increase in intermittency, which suggests the evolution of the flow process towards a state characterized by typical intermittency. A9 demonstrates a temporary decrease followed by an increase in the number of bubbles, suggesting that as the gas flow velocity increases, gas initially agglomerates and subsequently, intermittent liquid slugs cause bubble collision and rupture. A10 shows an increase, highlighting the widening distribution range of gas–liquid fluctuations. A11 serves as a local parameter attribute, indicating the continuous increase in gas flow velocity.

The characteristics of transition processes can be further analyzed by the class logits MM, which provides guidance for promptly determining the direction of evolution. The indication for transition Case #1 is presented in Fig. 10(b). The maximum class logits of the sampling points ranging from 1 to 85 surpass the established threshold, indicating that this stage exhibits characteristics of a typical flow state. Accordingly, it is identified as state 1. Conversely, the maximum class logits of the sampling points ranging from 86 to 511 fall below the threshold, signifying a transition stage. Finally, the maximum class logits for the sampling points from 512 to 600 once again exceed the threshold, indicating that the process has transitioned to a typical flow state, specifically identified as state 3.

Fig. 11 provides the detailed monitoring results for Case #2. In comparison with the monitoring results of Case #1, it is determined that the process is in an oil-based flow state. This process exhibits a flow state similar to that monitored in Case #1. However, during the transition stage, several samples are misidentified as state 8, where the interphase structure between gas and liquid is mistakenly recognized as plug. This misidentification can be attributed to the similarity in attributes between these samples.

In Fig. 12(a), attributes A1 and A2 describe the dominant phase as water globally. A3 indicates an increasing level of fluctuation intensity. A4 suggests an increase, indicating the gradual coexistence of multiscale structures. Attributes A5 and A6 indicate a transition from a separated to a dispersed interfacial structure between oil and water

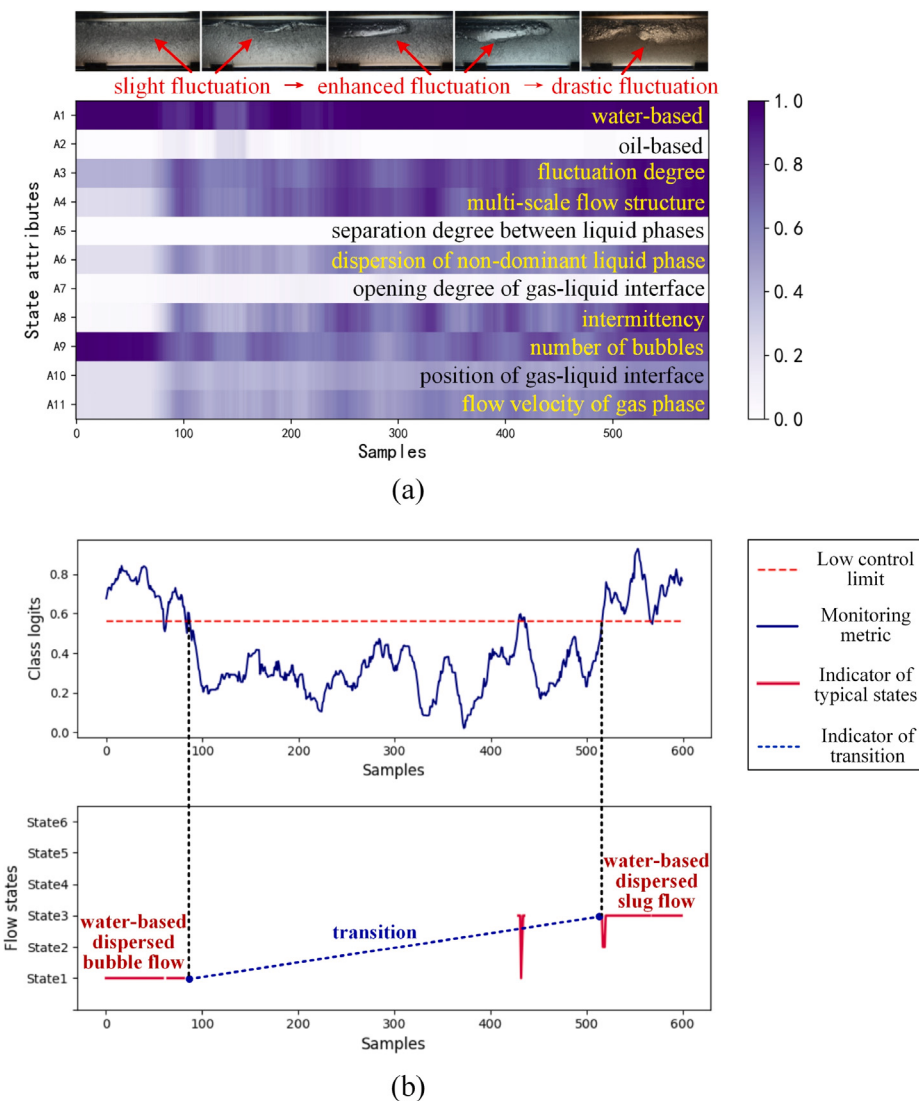


Fig. 10. Monitoring results for Case #1 by Ag-MRDCVA. (a) Attribute heat map, (b) Class logits MM.

in the flow process. A7 indicates a gradual decrease in the opening degree of the gas–liquid interface, accompanied by wave formation. A8 exhibits a gradual increase in intermittency, though it remains at a relatively low level. This points to the evolution of intermittent behavior in the flow process, particularly corresponding to the larger-amplitude rolls observed in the wave flow. A9 indicates an increasing number of gas bubbles. A10 increases that signifies a widening distribution range of gas–liquid fluctuations. A11 exhibits a continuous increase in the gas phase velocity.

In Fig. 12(b), the class logits MM of sampling points 1 to 236 are greater than the threshold, indicating that this stage represents a typical flow state classified as state 5. The class logits MM of sampling points 237 to 533 are smaller than the threshold, indicating the presence of a transition state. For sampling points 534 to 600, the class logits MM rise back above the threshold, suggesting that the process has transitioned to a typical three-phase flow state identified as state 4.

In previous researches, the transition states of industrial processes are often modeled as distinct states. However, for a three-phase flow process, such an approach may yield non-ideal monitoring results due to the similarities between the transition state and its adjacent typical flow states. By incorporating feature extraction and global-local attribute information from typical flow states, the model enables knowledge learning and transfer, as well as offers a fine-grained capture

of the state evolution during transition processes. This is a notable advantage, as the attribute information used in the model can be seen as a form of expert knowledge. Unlike traditional data-driven classification models that can be likened to black boxes, the descriptive nature of attribute information allows for a better understanding of the underlying mechanisms.

## 5. Conclusion

In this work, a novel method Ag-MRDCVA is proposed for monitoring oil–gas–water three-phase flow with nonlinear dynamic characteristics. It is the first time that the semantic attributes are designed with expert knowledge and introduced to describe the multiphase flow states. These semantic attributes serve as important auxiliary information, guiding the feature extraction process and providing meaningful explanations for effective process monitoring. The global serial correlation and local manifold structure are optimized simultaneously for information mining with the attribute guidance. Furthermore, an MM is designed integrating attributes and features to yield intuitive monitoring results, which can effectively indicate typical states and transition states. Meanwhile, the attribute heat maps offer comprehensive results and interpretable analysis. By combining feature extraction, global-local attribute information, knowledge learning and transfer,

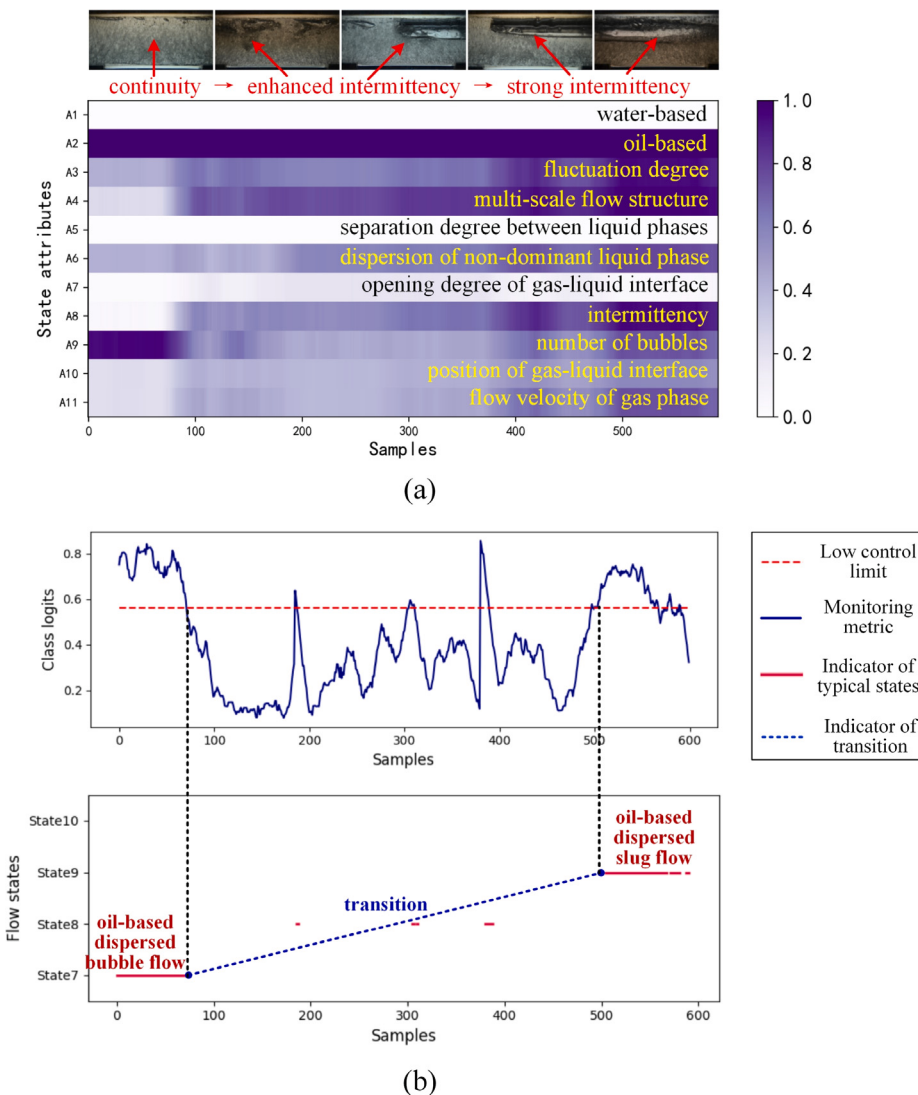


**Fig. 11.** Monitoring results for Case #2 by Ag-MRDCVA. (a) Attribute heat map, (b) Class logits MM.

the model provides a more comprehensive approach to monitor the transition process. It bridges the gap between empirical observations and theoretical understanding, making it a promising tool for process analysis, control, and optimization in various applications.

However, the proposed monitoring scheme does have certain limitations. Firstly, the Ag-MRDCVA primarily focuses on exploring temporal information through serial correlation and spatial information through manifold structure analysis. There exists additional domain knowledge related to attributes to explore. Secondly, although the chosen network backbone is straightforward and easy to deploy in hardware and industrial settings, its accuracy might be constrained compared to more complex models. Thirdly, the absence of a universally accepted definition for describing three-phase flow introduces subjectivity regarding the state attributes, necessitating further validation for objectivity.

Future researches could explore alternative DNNs and tuning methods to enhance feature representation abilities. Enriching feature-level information by incorporating process mechanisms and defining more objective attributes is suggested for future investigation. Moreover, knowledge about the description of the three-phase flow state can be embedded in the form of knowledge graphs, while mining the relationships between attributes. Given the demonstrated advantages of Ag-MRDCVA in learning deep representations for nonlinear dynamic processes and the knowledge transfer potential of semantic attributes,

the proposed method holds promise for applications in process monitoring across various industries, as well as ZSL and few-shot learning (FSL) scenarios.

#### CRediT authorship contribution statement

**Linghan Li:** Conceptualization, Methodology, Software, Writing – original draft, Writing – review & editing. **Feng Dong:** Methodology, Funding acquisition, Project administration, Writing – review & editing. **Shumei Zhang:** Supervision, Funding acquisition, Methodology, Validation, Writing – review & editing.

#### Declaration of competing interest

The authors declare that they have no known competing financial interests or personal relationships that could have appeared to influence the work reported in this paper.

#### Data availability

The authors do not have permission to share data.

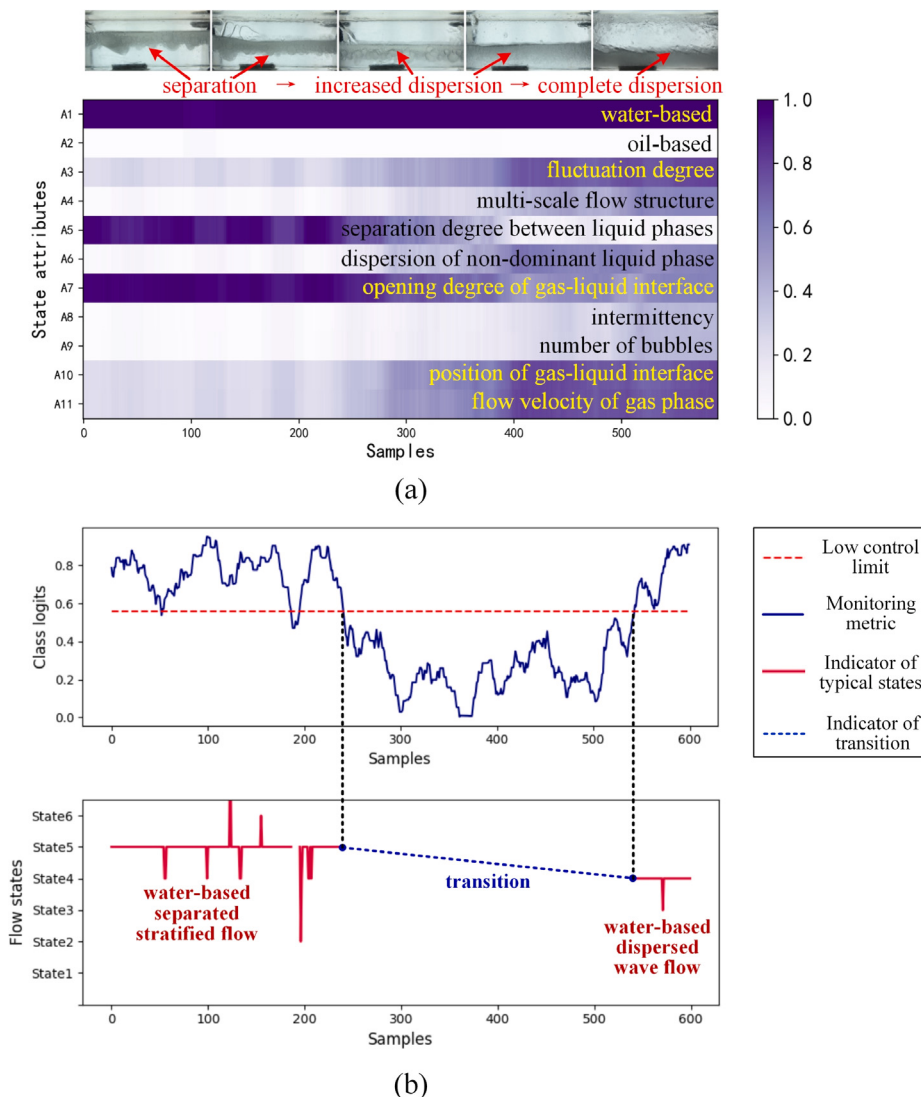


Fig. 12. Monitoring results for Case #3 by Ag-MRDCVA. (a) Attribute heat map, (b) Class logits MM.

## Acknowledgments

The authors would like to express their gratitude for the support from the National Natural Science Foundation of China (No. 62373277 and No. 51976137).

## References

- Açıkgoz, M., França, F. A., & Lahey, R. T. (1992). An experimental study of three-phase flow regimes. *International Journal of Multiphase Flow*, 18(3), 327–336.
- AL-Qutami, T. A., Ibrahim, R. B., Ismail, I., & Ishak, M. A. (2018). Virtual multiphase flow metering using diverse neural network ensemble and adaptive simulated annealing. *Expert Systems with Applications*, 93, 72–85.
- Chen, H., Li, L., Shang, C., & Huang, B. (2022). Fault detection for nonlinear dynamic systems with consideration of modeling errors: A data-driven approach. *IEEE Transactions on Cybernetics*, 53(7), 4259–4269.
- Chen, H., Luo, H., Huang, B., Jiang, B., & Kaynak, O. (2024). Transfer learning-motivated intelligent fault diagnosis designs: A survey, insights, and perspectives. *IEEE Transactions on Neural Networks and Learning Systems*, 35(3), 2969–2983.
- Chiplunkar, R., & Huang, B. (2021). Siamese neural network-based supervised slow feature extraction for soft sensor application. *IEEE Transactions on Industrial Electronics*, 68(9), 8953–8962.
- Dong, F., Wu, W., & Zhang, S. (2021). Flow state monitoring of gas-water two-phase flow using multi-Gaussian mixture model based on canonical variate analysis. *Flow Measurement and Instrumentation*, 79, Article 101904.
- Fallahdizcheh, A., & Wang, C. (2022). Transfer learning of degradation modeling and prognosis based on multivariate functional analysis with heterogeneous sampling rates. *Reliability Engineering & System Safety*, 223, Article 108448.
- Fang, X., Jiang, Y., Ji, H., Wang, B., & Huang, Z. (2024). A new CCERT system with shielding for gas-liquid two-phase flow. *IEEE Transactions on Industrial Electronics*, 71(4), 4241–4251.
- Fossa, M. (1998). Design and performance of a conductance probe for measuring the liquid fraction in two-phase gas-liquid flows. *Flow Measurement and Instrumentation*, 9(2), 103–109.
- Gao, Z., & Jin, N. (2011). Nonlinear characterization of oil-gas-water three-phase flow in complex networks. *Chemical Engineering Science*, 66(12), 2660–2671.
- Guan, S., Zhuang, Z., Tao, H., Chen, Y., Stojanovic, V., & Paszke, W. (2023). Feedback-aided PD-type iterative learning control for time-varying systems with non-uniform trial lengths. *Transactions of the Institute of Measurement and Control*, 45(11), 2015–2026.
- He, X., & Niyogi, P. (2003). Locality preserving projections. In *Neural information processing systems*.
- Kingma, D. P., & Ba, J. (2014). Adam: A method for stochastic optimization. arXiv preprint.
- Kuang, B., Nnabuike, S. G., Whidborne, J. F., Sun, S., Zhao, J., & Jenkins, K. (2024). Self-supervised learning-based two-phase flow regime identification using ultrasonic sensors in an S-shape riser. *Expert Systems with Applications*, 236, Article 121414.
- Lampert, C. H., Nickisch, H., & Harmeling, S. (2009). Learning to detect unseen object classes by between-class attribute transfer. In *2009 IEEE conference on computer vision and pattern recognition* (pp. 951–958).
- Li, L., Dong, F., & Zhang, S. (2023). Adaptive spatio-temporal feature extraction and analysis for horizontal gas-water two-phase flow state prediction. *Chemical Engineering Science*, 268, Article 118434.

- Liang, G., Kolehmainen, V., Vauhkonen, M., & Dong, F. (2023). Structural similarity driven joint reconstruction of conductivity and sound speed in EIT/UTT dual-modality tomography. *Inverse Problems*, 39(10), Article 105010.
- Lou, S., Yang, C., Zhang, X., Zhang, H., & Wu, P. (2023). From complexity to clarity: M2KCSVA's nonlinear temporal correlation analysis and stationary estimation pave the way for fault diagnosis in ironmaking processes. *IEEE Transactions on Industrial Informatics*, <http://dx.doi.org/10.1109/TII.2023.3333841>, early access.
- Muradore, R., & Fiorini, P. (2012). A PLS-based statistical approach for fault detection and isolation of robotic manipulators. *IEEE Transactions on Industrial Electronics*, 59(8), 3167–3175.
- Nnabuife, S. G., Kuang, B., Whidborne, J. F., & Rana, Z. A. (2021). Development of gas-liquid flow regimes identification using a noninvasive ultrasonic sensor, belt-shape features, and convolutional neural network in an S-shaped riser. *IEEE Transactions on Cybernetics*, 53(1), 3–17.
- Odiouei, P.-E. P., & Cao, Y. (2010). Nonlinear dynamic process monitoring using canonical variate analysis and kernel density estimations. *IEEE Transactions on Industrial Informatics*, 6(1), 36–45.
- Ojima, S., Hayashi, K., Hosokawa, S., & Tomiyama, A. (2014). Distributions of void fraction and liquid velocity in air-water bubble column. *International Journal of Multiphase Flow*, 67, 111–121.
- OuYang, L., Jin, N., & Ren, W. (2022). A new deep neural network framework with multivariate time series for two-phase flow pattern identification. *Expert Systems with Applications*, 205, Article 117704.
- Peng, C., Li, Z., Wang, G., & Pu, W. (2020). An effective deep recurrent network with high-order statistic information for fault monitoring in wastewater treatment process. *Expert Systems with Applications*, 167, Article 114141.
- Pilarino, K. E. S., Cao, Y., & Shafiee, M. (2019). Mixed kernel canonical variate dissimilarity analysis for incipient fault monitoring in nonlinear dynamic processes. *Computers and Chemical Engineering*, 123, 143–154.
- Puli, V. K., Raveendran, R., & Huang, B. (2021). Complex probabilistic slow feature extraction with applications in process data analytics. *Computers and Chemical Engineering*, 154, Article 107456.
- Rezaee, K., Zadeh, H. G., Chakraborty, C., Khosravi, M. R., & Jeon, G. (2023). Smart visual sensing for overcrowding in COVID-19 infected cities using modified deep transfer learning. *IEEE Transactions on Industrial Informatics*, 19(1), 813–820.
- Ruiz-Carcel, C., Cao, Y., Lao, L., & Samuel, R. T. (2015). Statistical process monitoring of a multiphase flow facility. *Control Engineering Practice*, 42, 74–88.
- Shi, X., Tan, C., Dong, F., & Escudero, J. (2022). Flow rate measurement of oil-gas-water wavy flow through a combined electrical and ultrasonic sensor. *Chemical Engineering Journal*, 427, Article 131982.
- Shi, X., Tan, C., Wu, H., & Dong, F. (2021). An electrical and ultrasonic Doppler system for industrial multiphase flow measurement. *IEEE Transactions on Instrumentation and Measurement*, 70, Article 7500313.
- Song, X., Wu, N., Song, S., Zhang, Y., & Stojanovic, V. (2023). Bipartite synchronization for cooperative-competitive neural networks with reaction-diffusion terms via dual event-triggered mechanism. *Neurocomputing*, 550, Article 126498.
- Stahl, P., & von Rohr, P. R. (2004). On the accuracy of void fraction measurements by single-beam gamma-densitometry for gas-liquid two-phase flows in pipes. *Experimental Thermal and Fluid Science*, 28(6), 533–544.
- Su, Q., Tan, C., & Dong, F. (2018). Measurement of oil-water two-phase flow phase fraction with ultrasound attenuation. *IEEE Sensors Journal*, 18(3), 1150–1159.
- Wang, X., Wu, P., Huo, Y., Zhang, X., Liu, Y., & Wang, L. (2022). Data-driven fault detection of a 10 MW floating offshore wind turbine benchmark using kernel canonical variate analysis. *Measurement Science & Technology*, 34(3), Article 034001.
- Wen, X., & Xu, Z. (2021). Wind turbine fault diagnosis based on reliefF-PCA and DNN. *Expert Systems with Applications*, 178, Article 115016.
- Wu, P., Lou, S., Zhang, X., He, J., Liu, Y., & Gao, J. (2021). Data-driven fault diagnosis using deep canonical variate analysis and Fisher discriminant analysis. *IEEE Transactions on Industrial Informatics*, 17(5), 3324–3334.
- Xu, X., & Ding, J. (2021). Decentralized dynamic process monitoring based on manifold regularized slow feature analysis. *Journal of Process Control*, 98, 79–91.
- Xu, Y., Zuo, R., Yuan, C., Liu, J., Li, T., Chen, X., & Fang, L. (2023). A water volume fraction measurement method based on flow regime insensitivity-microwave resonant cavity sensor (FRI-MRCS). *IEEE Sensors Journal*, 23(18), 21226–21233.
- Yang, J.-F., Zhang, N., He, Y.-L., Zhu, Q.-X., & Xu, Y. (2024). Novel dual-network autoencoder based adversarial domain adaptation with wasserstein divergence for fault diagnosis of unlabeled data. *Expert Systems with Applications*, 238, Article 122393.
- Yu, W., Wu, M., Huang, B., & Lu, C. (2022). A generalized probabilistic monitoring model with both random and sequential data. *Automatica*, 144, Article 110468.
- Yu, W., Zhao, C., & Huang, B. (2021). MoniNet with concurrent analytics of temporal and spatial information for fault detection in industrial processes. *IEEE Transactions on Cybernetics*, 52(8), 8340–8351.
- Zhai, L., Jin, N., Gao, Z., Zhao, A., & Zhu, L. (2014). Cross-correlation velocity measurement of horizontal oil-water two-phase flow by using parallel-wire capacitance probe. *Experimental Thermal and Fluid Science*, 53, 277–289.
- Zhan, H., Lin, J., Ak, K. E., Shi, B., Duan, L.-Y., & C. Kot, A. (2022). A<sup>3</sup>-FKG: Attentive attribute-aware fashion knowledge graph for outfit preference prediction. *IEEE Transactions on Multimedia*, 24, 819–831.
- Zhu, Y., Min, W., & Jiang, S. (2021). Attribute-guided feature learning for few-shot image recognition. *IEEE Transactions on Multimedia*, 23, 1200–1209.